PROCEEDINGS A

rspa.royalsocietypublishing.org

Research

Cite this article: Fannon JS, Fowler AC, Moyles IR. 2017 Numerical simulations of drumlin formation. *Proc. R. Soc. A* **473**: 20170220.
http://dx.doi.org/10.1098/rspa.2017.0220

Received: 27 March 2017
Accepted: 27 July 2017

Subject Areas:
glaciology, mathematical modelling

Keywords:
drumlins, ribbed moraine, mega-scale glacial lineations, instability

Author for correspondence:
A. C. Fowler
e-mail: andrew.fowler@ul.ie

Electronic supplementary material is available online at https://dx.doi.org/10.6084/m9.figshare.c.3850921.

THE ROYAL SOCIETY PUBLISHING

Numerical simulations of drumlin formation

J. S. Fannon[1], A. C. Fowler[1,2] and I. R. Moyles[1]

[1]MACSI, University of Limerick, Limerick, Ireland
[2]OCIAM, University of Oxford, Oxford, UK

ACF, 0000-0002-2062-6372

We summarize the present form of the instability theory for drumlin formation, which describes the coupled subglacial flow of ice, water and sediment. This model has evolved over the last 20 years, and is now at the point where it can predict instabilities corresponding to ribbed moraine, drumlins and mega-scale glacial lineations, but efforts to provide numerical solutions of the model have been limited. The present summary adds some slight nuances to previously published versions of the theory, notably concerning the constitutive description of the subglacial water film and its flow. A new numerical method is devised to solve the model, and we show that it can be solved for realistic values of most of the parameters, with the exception of that corresponding to the water film thickness. We show that evolved bedforms can be three-dimensional and of the correct sizes, and we explore to some extent the variation of the solutions with the model's parameters.

1. Introduction

Drumlins are small ovoid hills which are formed under ice sheets. They occur in swarms, and are somewhat analogous to aeolian dunes or water waves; equivalently, they may be thought of as occurring as the result of an instability of a state of uniform flow [1–4], although this view is by no means universally accepted [5–15]. After the retreat of the ice sheets following the last ice age, much of the former subglacial topography has been exposed, revealing the widespread presence of drumlins [16] (figure 1).

Historical studies of drumlins date back more than 200 years [17–22], and more recent significant developments are due to Smalley & Unwin [23], Boulton [24] and Menzies [25,26]. Much of the literature concerns the issue of whether drumlins are 'erosional'

Figure 1. A view from Westport Harbour, Co. Mayo, Ireland, of some of the drumlins of Clew Bay. (Online version in colour.)

or 'depositional', ignoring the problem of describing how the topography of drumlinized terrain actually arises, despite this being its most obvious feature [3].

Drumlins may be a part of a family of subglacial bedforms which includes ribbed moraine and glacial lineations (including MSGLs—mega-scale glacial lineations), and it is possible that they are all formed by a similar mechanism, with the differences being due to different ice flow conditions [27,28]. Indeed, this appears consistent with the instability theory [29], which is one of several theories [2,4,30] which has a viable quantitative (as opposed to descriptive) basis.

The instability theory in its most recent form treats the coupled subglacial flow of ice, water and sediment in the vicinity of the bed of an ice sheet. From its earliest statement by Hindmarsh [31] and Fowler [32], this theory has been developed in a sequence of papers [29,33–37], and has now reached a reasonable state of maturity, which we develop a little further in this paper. It has been used to predict the formation of ribbed moraine [38], as well as to explain the various forms of internal architecture which have been observed [39].

However, the development of this theory to a state where computations can reveal the full development of the subglacial landscape is hindered by its complexity. It is very difficult technically to construct a numerical method to solve the problem, although some efforts have been moderately successful [34,38]. Since the introduction of a dynamic description of water flow to the theory [35,36], however, no such computational method has yet proved viable.

The theory of subglacial geomorphology shares this shortcoming with its subaerial counterpart, where the classic theory of landscape development [40], formulated as a set of partial differential equations, led to hybrid numerical methods [41], which were eventually abandoned in favour of lattice-based models [42,43]. These are successful in a kind of fashion, but they retain a philosophical element of curve-fitting, and need to be treated with caution.

Very recently, Barchyn *et al*. [44] have applied the same idea to subglacial bedforms, concluding in particular that the range of observed bedforms (ribs, drumlins, MSGLs) can all be produced from the same model by adjustment of parameters. Having said that, their model mechanisms are subject to criticism, insofar as they do not appear to reflect the physically appropriate processes involving water and sediment transport.

Our purpose in this paper is to develop a numerical method to solve the instability model in its most recent mature form. We, therefore, begin by recapping the present state of this theory, providing at the same time a gloss on some inaccuracies that remained in the version of Fowler & Chapwanya [29].

2. The instability theory

The instability theory has been developed from its initial formulation over a number of years. The most recent incarnation is by Fowler & Chapwanya [29], to which further explanatory reference may be made. Because of the development of this theory over a period of almost 20 years, it will be difficult to grasp for the reader new to the subject. We therefore begin by providing a synopsis of the theory. Table 1 provides a listing of the principal variables of the model, and table 2 lists the physical parameters. Other derived quantities are given in tables 3 and 4.

There are three constituent parts to the formulation of the theory, and we treat these in turn.

(a) Ice flow

Ice is assumed to flow as a viscous fluid with constant viscosity over a deformable substrate (water-saturated till), on which it exerts a dimensional basal shear stress τ_b which generates a sliding velocity through a sliding law which also depends on the effective normal stress N at the ice/till interface. The elevation of the till surface is b, the elevation of the basal ice surface is $s \geq b$ and the intervening space is occupied by water, either in the form of a clast-filled water film [45], or as stream or cavity flow. The situation is illustrated in figure 2.

There are a number of length scales in the problem which are used to non-dimensionalize the model. These are the ice sheet depth d_i, the drumlin elevation scale d_D (which is used to scale both s and b), the till deformation scale d_T and the drumlin length scale l. The latter are given by

$$d_D = \frac{\tau_b}{\Delta\rho_{wi} g}, \quad d_T = \frac{\tau_b}{\Delta\rho_{sw} g(1-\phi)} \quad \text{and} \quad l = \left(\frac{\eta_i u_0 d_D}{\tau_b}\right)^{1/2} = \left(\frac{\eta_i u_0}{\Delta\rho_{wi} g}\right)^{1/2}, \tag{2.1}$$

where u_0 is the velocity scale, defined below. The density differences are defined by

$$\Delta\rho_{wi} = \rho_w - \rho_i \quad \text{and} \quad \Delta\rho_{sw} = \rho_s - \rho_w, \tag{2.2}$$

with $\rho_{s,w,i}$ being the sediment particle/water/ice density. Two important dimensionless parameters are the aspect ratio ν and corrugation parameter σ, and these are defined by

$$\nu = \frac{d_D}{l} \quad \text{and} \quad \sigma = \frac{l}{d_i}. \tag{2.3}$$

There is a uniform state which is a simple shear flow over a flat bed with uniform till thickness; the sliding velocity in this uniform state is u_0, which is the velocity scale used in (2.1). For small undulations ($\nu \ll 1$) in the ice/till interface (as we observe), the ice velocity is only weakly perturbed, and as a result the ice flow problem becomes an entirely linear one which can be solved by the Fourier transform.

When this is done, we find that the (dimensionless) kinematic boundary condition for the ice (also known as the closure condition) is

$$w = \alpha s_t + \bar{u} s_x, \tag{2.4}$$

where

$$\alpha = \frac{d_T}{d_D} \equiv \frac{\Delta\rho_{wi}}{\Delta\rho_{sw}(1-\phi)} \tag{2.5}$$

and additionally $\bar{u}$ (the dimensionless sliding velocity) is defined by

$$\overline{f(\bar{u}, N)} = 1. \tag{2.6}$$

Here, $f(\bar{u}, N)$ is the dimensionless basal stress at the ice/till interface, the overline denotes a spatial average (so $\bar{u}$ is a function of time only), and this condition represents a balance between the drag at the bed and the basal stress due to the overlying ice flow.

Table 1. The principal variables of the model and their meaning. The parameters of the model are listed in table 2. Listings of the dimensional scales and dimensionless parameters are provided in tables 3 and 4.

symbol	meaning
A	deformable till thickness
b	sediment surface
B	bedload transport function
$f(\bar{u}, N)$	dimensionless basal stress (sliding law)
F	basal stress perturbation
h	water film thickness
$J\,(\hat{J})$	convolution ice flow function (transform), (2.10)
$\mathbf{k}$	wavevector
$L\,(\hat{L})$	convolution ice flow function (transform), (2.10)
N	effective pressure
q	groundwater flux
s	basal ice surface
$\bar{u}$	dimensionless ice velocity
w	vertical ice velocity
W	basal water source (from till)
Γ	basal water source
Π	till effective pressure
τ_b	basal shear stress
$\boldsymbol{\tau}_\mathrm{e}$	effective bed stress
Φ	ice normal stress

The normal velocity w in (2.4) is given by

$$w = J * \Phi + L * F, \tag{2.7}$$

where $*$ denotes the Fourier convolution,

$$F = f(\bar{u}, N) - 1, \tag{2.8}$$

F is the basal stress perturbation, Φ is the ice normal stress and the Fourier transform of a function is defined by

$$\hat{f}(\mathbf{k}) = \int_{-\infty}^{\infty}\int_{-\infty}^{\infty} f(x,y)\,\mathrm{e}^{\mathrm{i}k_1 x}\,\mathrm{e}^{\mathrm{i}k_2 y}\,\mathrm{d}x\,\mathrm{d}y, \tag{2.9}$$

where $\mathbf{k} = (k_1, k_2)$ and

$$\hat{J} = \frac{\sinh^2 j}{2k(j + \cosh j \sinh j)} \quad \text{and} \quad \hat{L} = \frac{\mathrm{i}k_1 j}{2k^2(j + \cosh j \sinh j)}, \quad j = \frac{k}{\sigma}. \tag{2.10}$$

Note that $\hat{J}$ is bounded at $k = 0$, specifically

$$\hat{J}(0) = \frac{1}{4\sigma}. \tag{2.11}$$

The term in L is ignored, on the basis that it is small when j is large.

Table 2. The principal parameters of the model and their meaning.

symbol	meaning
d_i	ice sheet depth
D_s	sediment grain size
g	gravitational acceleration
k	till permeability
l_i	ice sheet extent (scale)
l_c^*	critical clast spacing
q_b	bedload transport scale
u_0	ice velocity
$\Delta\rho_{sw}$	$\rho_s - \rho_w$
$\Delta\rho_{wi}$	$\rho_w - \rho_i$
η_i	ice viscosity
η_s	till viscosity
η_w	water viscosity
ρ_i	ice density
ρ_w	water density
ϕ	sediment porosity
ψ	hydraulic head

Table 3. Derived values of scales.

symbol	meaning	typical value
d_D	drumlin elevation	11 m
d_T	till deformation depth	1 m
h_0	water film thickness	6 mm
l	drumlin length	640 m
l_i	ice sheet horizontal length scale	10^3 km
h_c	critical clast size	0.1 m
N_0	film-free effective pressure	10^6 Pa
t_D	time scale	74 years
Γ	melt rate	3 mm yr^{-1}
τ_b	basal shear stress	0.9×10^4 Pa

(b) Water flow

We discuss water flow in greater detail than ice flow, because our previous theory is elaborated. Slow water flow through a thin film or stream of depth h is given by a local Poiseuille flow and takes the dimensional form

$$h_t = \nabla \cdot \left[\frac{h^3}{12\eta_w} \nabla\psi \right] + \Gamma + W, \tag{2.12}$$

where ψ is the hydraulic head, η_w is water viscosity and Γ is the local water source due to internal melting in the ice.

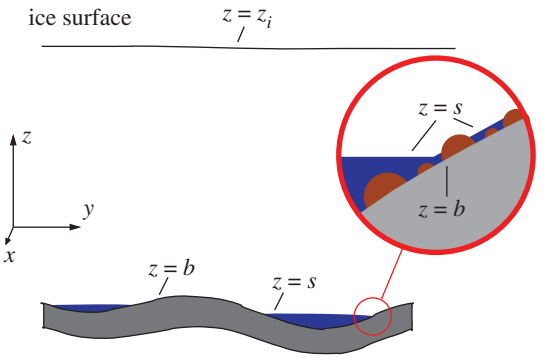

Figure 2. Illustration of the geometry of the problem. (Online version in colour.)

Table 4. Approximate dimensionless parameter values. The 'interpretation' means that the parameter can be thought of as a measure of the size of the indicated quantity.

symbol	typical value	interpretation
α	0.09	ice flow time scale
β	1.04×10^{-3}	till squeezing
γ	0.3×10^{-2}	stream bedload
δ	0.54×10^{-3}	water film thickness
ε	2.7×10^{-2}	film flow time scale
θ	0.62	downslope component of stream stress
λ	0.15	variation of film thickness with effective pressure
μ	0.6	granular friction coefficient
ν	1.7×10^{-2}	drumlin roughness (aspect ratio)
σ	0.64	drumlin corrugation (length/ice depth)
ω	0.41×10^{-6}	meltwater source
Ω	0.01	pore water suction from till

The term W represents the net source of water to the film from the underlying saturated till, and is a new development in the theory. The reason for this flux is that if a cavity forms (h becomes large), then water to fill it must be sucked from the till, which will cause a decrease of b, compaction and an increase in till effective pressure. Fowler [34] assumed that forming cavities would be rapidly infilled by upwards squeezing of the sediment, but did not concern himself with the consequence for water flow (which was only superficially described in that version of the theory). We now remedy that shortcoming.

We suppose that changes in b cause a primarily vertical flux of groundwater in the till, described by the conservation law

$$\phi_t + q_z = 0, \tag{2.13}$$

where $\phi(\Pi)$ is the porosity of the till, which is a decreasing function of the effective pressure Π within the till, and the Darcy flux q is given by

$$q = \frac{k}{\eta_w}\left\{\frac{\partial \Pi}{\partial z} + \Delta\rho_{sw} g(1-\phi)\right\}. \tag{2.14}$$

The boundary conditions for the flow are

$$\left.\begin{aligned} q &= 0 \quad \text{at } z = 0, \\ \text{and} \qquad \Pi &= N \quad \text{at } z = b. \end{aligned}\right\} \tag{2.15}$$

If we suppose that ϕ' (the prime denotes the derivative with respect to Π) is sufficiently small that the flow response time is small [35], then the water pressure is approximately hydrostatic, q is small and, if ϕ does not vary too much,

$$\Pi \approx N + \Delta\rho_{\mathrm{sw}} g(1-\phi)(b-z). \tag{2.16}$$

Of interest is the water flux from the till to the film above. To calculate this, we integrate (2.13) from 0 to b. Using (2.16), we find

$$q_{\mathrm{b}} \equiv q|_{z=b} \approx |\phi'| b \Pi_{\mathrm{t}} = |\phi'| b\{N_{\mathrm{t}} + \Delta\rho_{\mathrm{sw}} g(1-\phi) b_{\mathrm{t}}\}. \tag{2.17}$$

Now, exact integration of (2.13) from 0 to b shows that the net flux W from the till to the water film is

$$W = -\frac{\mathrm{d}}{\mathrm{d}t}\int_0^b \phi \,\mathrm{d}z = q_{\mathrm{b}} - \phi|_b \, b_{\mathrm{t}} \tag{2.18}$$

and thus

$$W = |\phi'| b N_{\mathrm{t}} - \{\phi - |\phi'| \Delta\rho_{\mathrm{sw}} g(1-\phi) b\} b_{\mathrm{t}}. \tag{2.19}$$

As a simple approximation, we will take

$$W \approx -\phi b_{\mathrm{t}}. \tag{2.20}$$

We scale equation (2.12) using the drumlin time scale

$$t_{\mathrm{D}} = \frac{d_{\mathrm{D}} l}{d_{\mathrm{T}} u_0} \equiv \frac{\Delta\rho_{\mathrm{sw}}(1-\phi) l}{\Delta\rho_{\mathrm{wi}} u_0} \tag{2.21}$$

and, in addition,

$$\psi \sim \tau_{\mathrm{b}}, \quad h \sim h_0 \quad \text{and} \quad W \sim \frac{\phi d_{\mathrm{D}}}{t_{\mathrm{D}}} = \frac{\phi d_{\mathrm{T}} u_0}{l}. \tag{2.22}$$

This leads us to the dimensionless form

$$\varepsilon\omega h_{\mathrm{t}} = \boldsymbol{\nabla}\cdot[h^3 \boldsymbol{\nabla}\psi] + \omega - \Omega b_{\mathrm{t}}, \tag{2.23}$$

in which the dimensionless hydraulic head is

$$\psi = -\sigma x + s - N + \Phi. \tag{2.24}$$

The definitions of the parameters assume a mean film thickness[1]

$$h_0 = \left(\frac{12\eta_{\mathrm{w}} l_{\mathrm{i}} l \Gamma}{\tau_{\mathrm{b}}}\right)^{1/3}, \tag{2.25}$$

where l_{i} is the horizontal ice sheet scale, and then

$$\varepsilon = \frac{h_0}{\Gamma t_{\mathrm{D}}}, \quad \omega = \frac{l}{l_{\mathrm{i}}} \quad \text{and} \quad \Omega = \frac{\phi d_{\mathrm{T}} u_0}{\Gamma l_{\mathrm{i}}}. \tag{2.26}$$

While this gives a way to accommodate suction of water from, or expulsion to, the underlying sediment, we shall later find that $\Omega \ll 1$ so that in practice it is unimportant.

[1]Note that (2.32) of Fowler & Chapwanya [29] contains an error, corrected here, although the inferred value of h_0 in table 2 of that paper is correct.

(c) Sediment flow

Sediment flow is described by the Exner equation, which takes the dimensionless form

$$b_t + \bar{u}A_x = \beta \boldsymbol{\nabla} \cdot [A^3 \boldsymbol{\nabla} N] - \gamma \boldsymbol{\nabla} \cdot [B(\tau_e)\boldsymbol{\tau}_e], \tag{2.27}$$

where the dimensionless parameters are defined by Fowler & Chapwanya [29] as

$$\beta = \frac{2d_T^2 \tau_b}{3\eta_s l u_0} \quad \text{and} \quad \gamma = \frac{q_b}{d_T u_0}, \tag{2.28}$$

where η_s is an assumed sediment viscosity and q_b is a bedload transport scale. These quantities are discussed further below. The choice of time scale in (2.27) was given in (2.21).

The fluxes comprise three terms. The first, $\bar{u}A\mathbf{i}$, represents the advection of till by the ice flow. The assumption is that the ice grips the till and drags it along as a shear flow. The quantity A is the dimensionless deformable till thickness, which is a function of the overlying shear stress τ and the effective pressure at the ice/till interface N:

$$A = \frac{1}{2}\left[\frac{\tau}{\mu} - N\right]_+, \quad \tau = f(\bar{u}, N). \tag{2.29}$$

It is a unimodal (one-humped) function of N because it is determined by the yield stress of the till, which allows deformation. As N increases, the till becomes stiffer, which reduces A, but this is offset at small N by the fact that the driving stress itself increases with N. It is the fact that A increases with N at small N that enables the ribbing part of the instability to occur.

The first term on the right-hand side of (2.27) is the till-squeezing term. It indicates that the till will be squeezed down effective pressure gradients, in keeping with Terzaghi's principle that the deformation of saturated granular materials (soils) is determined by the effective pressure. It is a stabilizing term. The parameter β involves an assumed till viscosity. As a granular material, till has a yield stress, but this does not help in choosing a rheology, and a viscous flow law (with viscosity being such as to remain on the yield surface) is a straightforward choice, although the reality of the matter is doubtless more complicated. As we can expect $\tau_b \sim (\eta_s u_0/d_T)$, we see that

$$\beta \sim \frac{d_T}{l} \tag{2.30}$$

and is small.

The second term on the right-hand side of (2.27) represents the bedload transport of sediment by stream flow. By $\boldsymbol{\tau}_e$, we denote the effective bed stress due to water flow which drives the transport, and it is given dimensionlessly by

$$\boldsymbol{\tau}_e = -h\boldsymbol{\nabla}\psi - \theta\boldsymbol{\nabla}b, \tag{2.31}$$

where

$$\theta = \frac{2\Delta\rho_{sw} D_s}{\Delta\rho_{wi} h_0}; \tag{2.32}$$

here D_s is the sediment grain size. The bedload transport function B is an increasing function of τ_e. A comment on this function is necessary. The normal scale of water film thickness is of the order of millimetres, and the flow is so slow that only the smallest particles might be moved; therefore, it seems inappropriate to use a stream-based recipe as we do. On the other hand, we know that subglacial streams do occur, and indeed that floods occur between subglacial lakes, and from subglacial lakes to the ice sheet margin [46–48], so some mechanism to form streams must exist. Given this, we associate the transport by bedload with the irregular occasions when a viable stream system exists. However, we do not expect such transport to occur all the time, but rather during occasional flood events (as indeed happens subaerially). This makes the choice of the bedload transport coefficient and the function B somewhat speculative. A typical stream flow choice is a power law $B = \tau_e^{m-1}$, where commonly $m = \frac{3}{2}$, but in the present situation this function should be based on flood frequency and magnitude, which are not simply related to the mean water film thickness. Similarly, γ in (2.28) represents the ratio of mean waterborne sediment

transport to till flux, and this also is very unconstrained. We estimate it as being small, but it is liable to be quite variable. Indeed, one can imagine situations where the till is very stiff, so that most transport is waterborne; in this case γ would be large. In our simulations, we use a value $m = 3.5$ (partly because we require $m > 3$ for the lineation instability).

The geometric relation between the ice base and the sediment floor is

$$b = s - \delta h, \tag{2.33}$$

where

$$\delta = \frac{h_0}{d_D} \tag{2.34}$$

and is present because the ice roof elevation and sediment floor elevation have a different scale (d_D) from that of the water film depth (h_0).

(d) Ice 'closure'

Counting equations, we see that (2.4), (2.6), (2.7), (2.8), (2.10), (2.23), (2.24), (2.27), (2.29), (2.31) and (2.33) provide 12 equations for the 13 unknowns w, s, $\bar{u}$, N, J, L, Φ, F, h, ψ, b, A and $\boldsymbol{\tau}_e$. An extra equation is necessary to close the system. In the classical stability theory [31,32], this is taken to be the condition of constant hydraulic potential, $\psi = -N_c$, but in the present context that is not enough, because we have explicitly introduced the water layer thickness h. Fowler [34] accommodated $h > 0$ (the formation of cavities) with the extra statement

$$\left.\begin{aligned} h &= 0 \quad \text{if } N > 0, \\ \text{and} \qquad N &= 0 \quad \text{if } h > 0 \end{aligned}\right\} \tag{2.35}$$

and required nothing else. Fowler & Chapwanya [29] modified this by including a closure equation of the form

$$\frac{\partial h}{\partial t} = \frac{\rho_w \Gamma}{\rho_i} - \frac{l_c^* N}{\eta_i N^*(h)}, \tag{2.36}$$

where Γ is the basal melting rate, l_c^* is a critical 'clast spacing' length scale of the rough till surface and $N^*(h)$ is a sharply decreasing function of h. In equilibrium, (2.36) provides a continuous approximation to (2.35), but its provenance is suspect, despite its resemblance to the classic Röthlisberger closure equation.

To see this, we recall that the Röthlisberger theory [49,50] consists of equations representing conservation of mass, momentum and energy for water flow in a semicircular conduit, which provide three equations for the four variables Q (volume flux), S (cross-sectional area), m (melting rate) and N (effective pressure), and the theory is completed by a closure equation. This apparently provides a second evolution equation for S, which makes the theory seem strange. In fact, this closure equation is determined by the viscous closure of the ice, and is actually a representation of the kinematic boundary condition of the ice flow.

Given this, our cause for concern in specifying (2.36) is that it presumably also represents a kinematic boundary condition for the ice flow; but we have already prescribed this in writing (2.4)! Although the two equations clearly represent processes at two different length scales, it is not clear how a single kinematic equation should be able to give rise to *two* equations. We, therefore, re-examine this issue.

We now take an alternative view. The till is a compressible porous medium with a porosity ϕ which, in the normal way of soil mechanics, is taken to be a decreasing function of the effective pressure in the till, $\phi = \phi(\Pi)$. In our discussion of the water film, we conceive of it as a discrete layer *lying within the upper surface of the till*. It is in fact a second porous layer of very small thickness. As such, its porosity ϕ_s can be taken to be a function of its effective pressure N. Further, it seems clear that the effective porosity of the surface should be an increasing function of the

film thickness. The consequence of all this is that we may take layer thickness to be a decreasing function of N,

$$h = G(N), \tag{2.37}$$

which mimics (2.36) but lacks the time derivative. As in our earlier work [29] this time derivative term was small, our stability results there remain valid.

In specifying a suitable form for $G(N)$, we introduce a *critical clast size* h_c, which is a measure of the coarseness of the till. Our concept of the water film is that of Creyts & Schoof [45], embedded as a water layer within the topmost clasts of the till, such that when its thickness exceeds h_c, then the ice loses its grip on the till and the effective pressure becomes zero. In reality, it is more likely that h_c represents the length scale over which N approaches zero.

As $h \to 0$, we suppose that the effective pressure should approach N_0, which would be the effective pressure necessary to evacuate the water flux entirely through the till. Any reasonable calculation suggests that this is very high. For example, evacuation of a vertical flux of 3 mm yr^{-1} to a canal at a distance of 10 km through a substrate of permeability 10^{-15} m^2 requires an effective pressure of $\sim 10^6$ Pa, calculated using Darcy's law: not unreasonable, but enormous in terms of typical effective pressures necessary to deform till.

If N changes by $O(N_0)$ when h changes by $O(h_c)$, then in dimensionless terms

$$-\frac{\partial N}{\partial h} \sim \frac{1}{\lambda}, \quad \lambda = \frac{\tau_b h_c}{N_0 h_0}, \tag{2.38}$$

because N is scaled with τ_b and h with h_0. In the absence of any further information, we take

$$\lambda h N = 1 \tag{2.39}$$

as a credible dimensionless candidate for this water film law. While this is mathematically more or less identical to the formulation of Fowler & Chapwanya [29], the physical description is quite different, and the definition of the corresponding parameter to λ (which was there denoted as Π) is quite different.

(e) A reduced model

Values of the constants used in scaling, and the values of the resulting dimensionless parameters, were estimated by Fowler & Chapwanya [29], and are summarized in tables 3 and 4. Many of the parameters are small, and we neglect some but retain others, as discussed below. A particular point concerns the magnitude and form of the waterborne sediment transport term. As mentioned following (2.32), this term uses standard assessments of bedload transport to estimate γ, but in fact the term can only have useful meaning during flood events or in localized stream flow, so the effective magnitude of γ and the form of the transport function $B(\tau_e)$ are not well constrained.

Although the model is complicated, its structure is relatively simple, as we now explain. The principal describing equations are the Exner equation (2.27) for b, the water mass equation (2.23) for $\psi = -\sigma x + \Psi$ and the ice flow kinematic condition (2.4) for s:

$$\left.\begin{aligned} b_t + \bar{u} A_x &= \beta \boldsymbol{\nabla} \cdot [A^3 \boldsymbol{\nabla} N] - \gamma \boldsymbol{\nabla} \cdot [B(\tau_e) \boldsymbol{\tau}_e], \\ \boldsymbol{\nabla} \cdot [h^3 \boldsymbol{\nabla} \Psi] &= \sigma (h^3)_x \\ \text{and} \qquad \alpha s_t + \bar{u} s_x &= J * \Phi, \end{aligned}\right\} \tag{2.40}$$

in which we suppose J is given by the inverse of $\hat{f}$ in (2.10). We have ignored the small terms in ω and Ω, but not those in β and γ in $(2.40)_1$. The term in β is a necessary stabilizing term, and will actually increase in magnitude as $N \to 0$, because then the till becomes much more fluid (although this is offset by the decrease in A). The term in γ allows the rilling instability associated with the formation of lineations via the production of stream flow. Thus, both of these terms are essential.

These equations for b and ψ introduce five subsidiary variables: A, N, $\boldsymbol{\tau}_e$, Φ and h. These are determined by the equations

$$\left.\begin{aligned} \Psi &= s - N + \Phi, \\ A &= \frac{1}{2}\left[\frac{f(\bar{u}, N)}{\mu} - N\right]_+, \\ \lambda h N &= 1, \\ b &= s - \delta h \\ \text{and} \qquad \boldsymbol{\tau}_e &= -h[\boldsymbol{\nabla}\Psi - \sigma \mathbf{i}]. \end{aligned}\right\} \tag{2.41}$$

We have neglected the term in θ on the basis that $\gamma\theta$ is small and the term in L in (2.7) on the basis that σ is relatively small (thus j is large), but we do not neglect δ because the term δh is singular; we actually use $(2.41)_4$ to determine h.

(f) Instability mechanisms

We now recall the instability mechanisms in the model [29]. The ribbing instability is due to the advective term in $(2.40)_1$, when $A'(N) > 0$; the mechanism is somewhat analogous to mechanisms of (transverse) dune formation, insofar as the maximum sediment transport is shifted upstream of the bed elevation maximum.

In more detail, Smith [51] and Engelund [52] were the first to show that the formation of aeolian or fluvial dunes due to the action of wind or water flow could be ascribed to the fact that the forming dunes altered the overlying (turbulent) fluid flow in such a way as to shift the maximum of the shear stress at the bed *upstream* of the maximum dune elevation; this was achieved by solving the approximating Orr–Sommerfeld equation for the disturbance to the flow. In consequence, the maximum sand transport is also shifted upstream, and a simple consideration of the Exner equation explains the resulting instability.

In this theory, the predominant transport of sediment is also presumed to be by its shear by the overlying ice. The instability is also due to this transport being maximal upstream of the bed elevation maximum, which is caused by an increase in the bed shear stress because of a presumed dependence of the sliding law on the effective pressure. It is not, however, an increase in the ice flow velocity which increases the till flux, but an increase of the deforming till depth (i.e. the depth to the critical yield stress where $N = \tau_b/\mu$). The instability mechanism is the same as that for dune formation, but for a somewhat different reason.

The lineation instability is due to the term in γ in $(2.40)_1$, and is analogous to the rilling instability of Smith & Bretherton [40]; in the present case, it requires the bedload function B to be sufficiently rapidly increasing: if we assume a power law $B \propto \tau_e^{m-1}$, then we require $m > 3$. In Smith and Bretherton's theory, regularization of the instability at high wavenumber is provided by the small term in δ in $(2.41)_4$ [53–55].

Physically, one can interpret this part of the instability mechanism as occurring because the formation of transverse ribs causes a pooling of water in the troughs, and one naturally expects such forming pools to be unstable and lead to downstream water flow. The distinction between the 'drumlin' and 'lineation' features that we exhibit below is essentially one of the amount of water and the efficiency with which it can transport sediment.

The term in β is stabilizing; thus all three derivative terms in $(2.40)_1$ are important to retain. In addition, the nonlinear coefficient h^3 features importantly in the stability analysis, particularly for lineations, but the coefficient h in $\boldsymbol{\tau}_e$ seems less significant.

3. Numerical solution

We aim to solve (2.40) and (2.41), assuming periodic boundary conditions on the boundaries of our square domain, which seems appropriate, given that this area represents a small segment

of a much larger bedform field. The function $A(N)$ is described by Fowler [34], and we have followed its approximation as given by Fowler [34] and Chapwanya *et al*. [38]. Efforts to solve such equations have previously used an entirely spectral approach [34,38], mainly because the convolution term in $(2.40)_3$ is most easily dealt with this way. This causes technical difficulties, however, because rapid changes in N cause the generation of high wavenumber components, and the requirement for N to remain positive provides a serious constraint on numerical implementation. Efforts to implement such a method for the version of the model given by Fowler & Chapwanya [29] failed entirely, however.

Here, we provide a different numerical method which appears to be relatively successful. It is based on time-stepping the equations for b and s, $(2.40)_1$ and $(2.40)_3$; we use finite differences to compute the spatial derivatives in the b equation, but a spectral method for the s equation. Both equations are integrated forwards using the method of lines.

Having stepped s and b forwards, $(2.41)_4$ determines h, $(2.41)_3$ then determines N, $(2.40)_2$ can be solved to determine Ψ and then $(2.41)_1$ gives Φ. We can then proceed to the next time step. We assume periodic boundary conditions in both x- and y-directions for s, b and Ψ.

For the initial conditions, we mostly assume small random perturbations about the base state $b=0$ and $s=\delta$; typically these are of dimensionless magnitude $\sim 10^{-3}$, corresponding to elevation variations of a few centimetres.

In solving for Ψ in $(2.40)_2$, central differencing is used for the nonlinear Laplacian, and a backward difference for the advective term. This yields a linear inhomogeneous matrix equation for the components of Ψ, but the matrix is singular, due to the fact that, with periodic boundary conditions, the solution of $(2.40)_2$ can only be determined up to addition of an arbitrary constant. To resolve this degeneracy, note that, by averaging $(2.40)_3$ over the domain, we obtain

$$\alpha\bar{s}_t = \frac{\bar{\Psi} + \bar{N} - \bar{s}}{4\sigma}, \tag{3.1}$$

using the periodicity of s, $(2.41)_1$ and (2.11). Additionally, we have $\bar{b}_t = 0$, whence we can take $\bar{b}$ to be constant and equal to its initial value, and therefore (3.1) leads to

$$4\sigma\alpha\delta\bar{h}_t = \bar{\Psi} + \frac{\overline{h^{-1}}}{\lambda} - \delta\bar{h} - \bar{b}. \tag{3.2}$$

With periodic boundary conditions, there is no net water flow into the domain, and consequently $\bar{h}_t = 0$. This would actually be a consequence of integrating (2.23) over the domain if we take the source term $\omega = 0$. However, it appears slightly worrying that if $\omega \neq 0$, then $\varepsilon\bar{h}_t = 1$. The issue is that the source is absorbed into an increase of water flux through the domain, so that exact periodicity is not required. With this proviso, we take $\bar{h}_t = 0$, and thus

$$\bar{\Psi} = \bar{b} + \delta\bar{h} - \frac{\overline{h^{-1}}}{\lambda}. \tag{3.3}$$

In differencing the b equation, we use flux-conservative central differences for the diffusion terms, but for the two convective terms (the term in A_x and that for $(Bh)_x$ in $\boldsymbol{\nabla}.[B\boldsymbol{\tau}_e]$) the expected sharp changes in N and thus h suggest upwinding, but it is not obvious in which direction this should be. To circumvent the issue, we have chosen to compute the first derivative terms spectrally; thus, for example,

$$A_x = \mathcal{F}^{-1}[-\mathrm{i}k_1\hat{A}], \tag{3.4}$$

where $\mathcal{F}$ is the Fourier transform. While this appears to give good results, it does rely on the use of periodic boundary conditions, and on the splitting technique applied.

In solving the problem numerically, we have found that, of the three critically small parameters β, γ and δ, the first two can be reduced satisfactorily without undue numerical issues, but the value of δ causes serious problems, as the solutions become increasingly singular, and we have not been able to obtain useful results for values of $\delta < 0.1$; obviously, this is a shortcoming of our method. More specifically, sharp changes in h occur, and, as found by Fowler [34] and Chapwanya

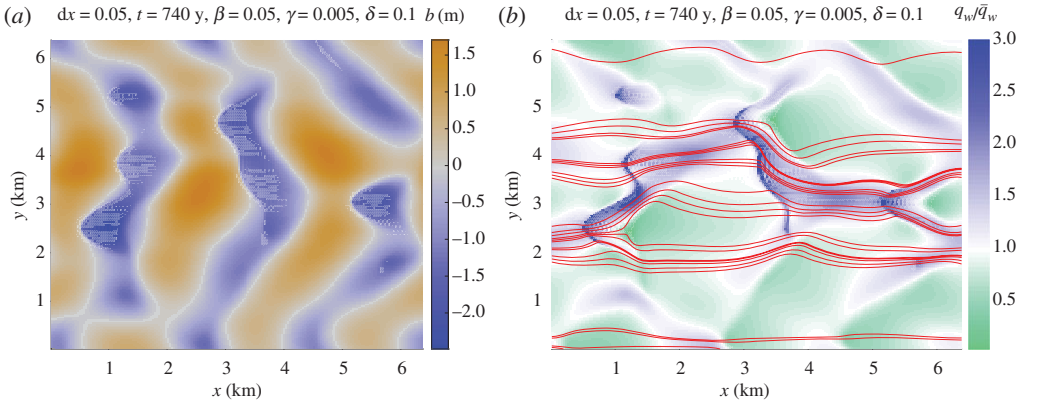

Figure 3. Rib-like features at $t = 740$ years. Parameter values $\delta = 0.1$, $\gamma = 0.005$, $\beta = 0.05$. (*a*) The topography, and (*b*) the water flux (as a fraction of the mean); green areas are essentially dry, and the red curves are streamlines for water flow, spaced with equal amounts of water flux between them. Essentially, the water makes its way over the topography, but there is evidence of streaming flow. The dimensionless box length and width is 10, and the dimensionless space step is 0.05, although the data are all plotted dimensionally.

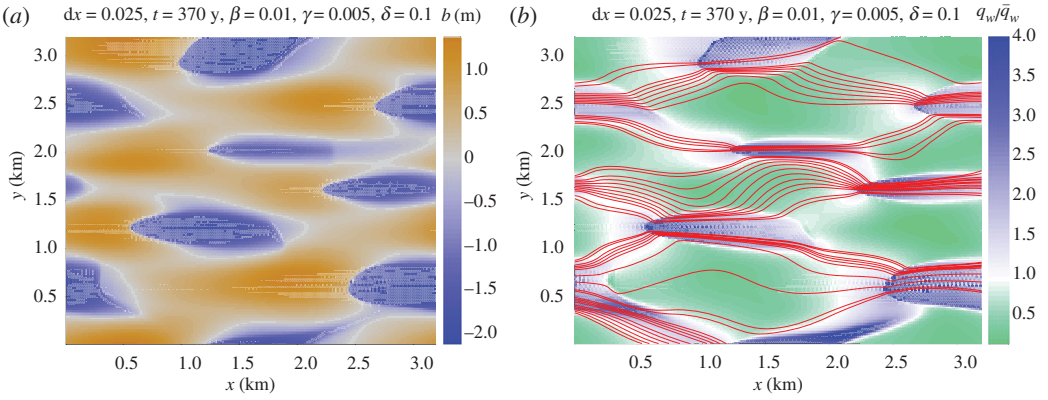

Figure 4. Drumlin-like features at $t = 370$ years. Parameter values $\delta = 0.1$, $\gamma = 0.005$, $\beta = 0.01$. The water flow begins to be concentrated in stream segments and to flow round the bedforms (*b*), while the bedforms are somewhat drumlin-like.

et al. [38], the spectral parts of the code cause Gibbs-like phenomena to occur. Unlike the latter paper, we have not resorted to filtering of high wavenumber components.

In the electronic supplementary material, we provide three fairly typical movies of the solutions through time with different choices of parameter values. In figures 3, 4 and 5, we show the final frame of these runs. During the course of the evolution of the bedforms with time, they typically are rib-like at early times, and they continue to evolve with time. Figure 3 shows bedforms which are somewhat rib-like, figure 4 shows three-dimensional structures analogous to drumlins and figure 5 resembles lineations, though it should be pointed out that the 'lineations' are inclined to the direction of ice flow (in the x-direction). Apart from the parameters in table 4, we use values $\lambda = 1$ and $m = 3.5$.

The lineations in figure 5 are inclined to the ice flow because there is a net lateral water flux. Our use of periodic boundary conditions allows this, and it seems admissible in the model. We think this odd occurrence is due to the assumption of a pathologically flat initial surface. In reality, there is always some topographic variation, and we might suppose that any lateral valley-like

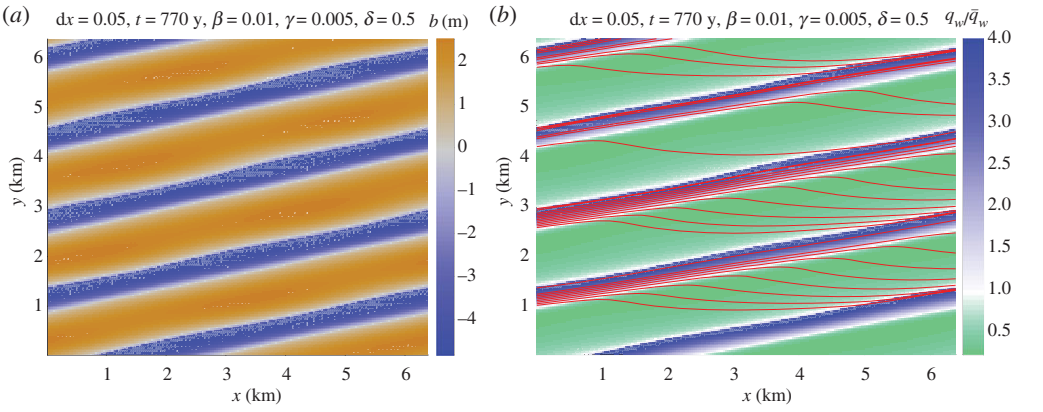

Figure 5. Lineation-like features at $t = 7770$ years. Parameter values $\delta = 0.5$, $\gamma = 0.005$, $\beta = 0.01$. The water flow is concentrated into streams between the lineations.

topography will act to confine the water flow in a local catchment, but we have not been able to provide a satisfactory numerical illustration of this.

In the figures (but not in the movies), we have included streamlines $\chi = \text{const.}$ representing water flow, where

$$\chi = \int q_1 \, dy - q_2 \, dx, \quad \mathbf{q} = (q_1, q_2). \tag{3.5}$$

Some interpretation of these is necessary. Firstly, the streamlines are not periodic in x, nor need they be. For example, the streamlines of $\chi = y - x$ are just a family of straight lines, but the velocity field is periodic.

Bunching of streamlines indicates streaming, and thus we see that, in figure 3, water begins to be focused in streams, while in the drumlin figure 4 water focuses in the depressions, which are in essence cavities, and flows round the elevations; finally in figure 5, stream flow is confined to the valleys between the lineations.

4. Discussion

(a) The model

A model is, of course, only that. But within the attempt to describe the physical processes, there are a great many assumptions which are made. Some of these are more critical than others; we now offer a commentary on some of them. That ice viscosity is Newtonian seems unlikely to be critical. Similarly with the assumption of an effectively viscous till. What is critical for till deformation is that $A(N)$ is a concave function of N, and this requires two things: no deformation below the yield stress, and a sliding law in which basal stress is an increasing function of N. While this is a common deduction in hard bed sliding laws, a precise derivation requires a presumption of till rheology, and such studies are not well advanced. On the other hand, the equivalent presumption that till becomes more deformable as effective pressure is reduced seems intuitively reasonable.

Of more concern is the way in which we model water flow. Firstly, the way in which the Creyts–Schoof water film is described by a relation between water depth and effective pressure is open to further scrutiny, and, more so than the sliding law, this 'water film law' is largely heuristic. This is important, because, as shown by Fowler & Chapwanya [29], its parametric form is critical to the form of the resulting instability.

Water flow, and accompanying sediment transport, is modelled as a continuous process but this cannot be the actual case. Sediment transport can only practically occur during floods and

does not occur continuously. While a continuous model nevertheless makes sense, it becomes unrealistic to model sediment transport using subaerial correlations. In particular, the size and frequency of floods will themselves depend on details of the water flow. For example, we might suspect that floods only occur for a sufficiently large water flux, and thus h. In this case, we would effectively have $B = 0$ for h less than some critical value, and increasing rapidly thereafter; in a power law $B \propto \tau_e^m$, this would correspond to a high value of m.

(b) Computations

The principal limitation of the computations is the inability to reduce δ to a sensibly small value. Small δ causes sharp changes in h, which can only be resolved by taking inordinately small space step sizes, which makes computation time (which is already long) prohibitive. Certainly, this is an issue for future study. It should be noted that the long times over which the bedforms evolve in the simulations are an artefact of the high values of δ used. In reality, we expect that, for smaller values, the time scales of bedform evolution will be nearer to decades.

(c) Comparison with linear stability results

Naturally, one wishes to compare the results with our earlier stability results [29]. Our results are indeed consistent, at least for the early growth phase, but the nonlinear evolution deviates from this, so that a comparison is not so straightforward.

The linear stability analysis of Fowler & Chapwanya [29] showed that variation of the parameter Π (from 0.7 to 10 in figure 4 of that paper) accounted for instability results corresponding to ribs, drumlins and MSGLs. While the model presented in this paper is a slight variant of this previous work, the stability results are analogous. In our case, the parameter λ now plays the role of Π, with λ in the range 1–15 demonstrating the same qualitative transition from ribs to MSGLs (in terms of linear stability results). Note that these stability results assume fixed values for β, γ and δ, as in Fowler & Chapwanya [29], and consistent with those in table 4.

Our approach in this paper has been orthogonal, as we have focused on the ability to obtain credible numerical results. The parameters we have used have, for this reason, not been the same as those in table 4; in particular, the value of δ used is much larger. For the three parameter combinations presented above, the linear stability analysis predicts the formation of ribs at early times, and indeed, this behaviour is seen in the movies in the electronic supplementary material. Beyond this initial linear growth phase, however, the bedforms evolve nonlinearly, and the differing outcomes are due to the different types of nonlinear evolution at these different parameter values.

(d) Results

The three figures indicate that a variety of bedforms can be produced, both by varying the parameters and also by looking at different times within one run. For example, the run which yields figure 5 shows drumlin-like behaviour at 4000 years, and rib-like bedforms earlier on. Despite such large time scales being a consequence of the artificially large value of δ used, the fact that bedforms may continue to evolve over time has an implication for any practical conclusions we might wish to make, because while we assume constant ice flow conditions in our simulations, it is likely that ice flow magnitude, basal shear stress and flow direction will all change in time, making the issue of prediction something of a free-for-all. While it is tempting to rush into such experiments, it may be advisable to await such time as confidence in the veracity of the model (not to mention the numerical computations) improves.

In the figures, we have plotted contours indicating stream flow, and it is noticeable that the flow becomes localized, consistent with the expectation of Kyrke-Smith & Fowler [37]. It is also found that the 'streams' remain of millimetric dimensions; large cavities do not form (or as they

do, they are infilled [34]), and we suppose that the millimetric stream thickness represents a time average of occasional flood events.

One comment we might make concerning the movies is that the initial instability occurs at smaller wavelengths than the later evolved bedforms. This behaviour is similar to that found by Chapwanya *et al*. [38], and is a common feature in many systems, particularly those involving granular flows [56], but our simulations do not indicate that the coarsening continues indefinitely.

(e) Criticisms

We mentioned in the Introduction that there are a number of other models in existence for bedform formation, although few of these are quantitatively based, but the promotion of other theories carries an implication that the instability theory may be unrealistic. We comment on two such criticisms.

Some time ago, Schoof [57,58] offered three objections to the instability theory, as it then existed. The first of these was that the instabilities were inherently two-dimensional, and could thus not explain drumlins. This led Dunlop *et al*. [33] to adopt a defensive position where they restricted their aim to the explanation of ribbed moraine. More recent work [29] indicates that this criticism is without foundation. Schoof also thought that the existence of internal stratification was inconsistent with the view of drumlins as travelling wave forms, but this view was rebutted by Stokes *et al*. [39], who indicated that internal stratification would be maintained in a net erosional environment. Finally, Schoof suggested that the onset of cavitation would restrict drumlin amplitudes in the instability theory to a few metres, although it turns out that such amplitudes are commonly observed [59]. Our present results, while not conclusive, are certainly consistent with this view, so this objection still has some merit.

A more recent challenge to the theory lies in the detailed observations of drumlins at Mulajökull by McCracken *et al*. [60]. These observations provide two results which, it is suggested, are inconsistent with the instability theory. The first is that till fabrics indicate till deformation by shear, which is supposed to be inconsistent with the instability theory assumption of compressive stresses. This objection appears to result from a misreading of the theory, which indeed yields instability via a negative flux divergence in the Exner equation (2.27), which can be written in the form

$$\left.\begin{aligned} b_{\mathrm{t}} &= -\boldsymbol{\nabla}.\mathbf{q}_{\mathrm{b}} \\ \text{and} \qquad \mathbf{q}_{\mathrm{b}} &= \bar{u}A\mathbf{i} - \beta A^3 \boldsymbol{\nabla} N + \gamma B \boldsymbol{\tau}_{\mathrm{e}}. \end{aligned}\right\} \tag{4.1}$$

The largest contribution is the ice-dragged till flux, which is indeed a shearing flow, and the negative divergence (upstream of a maximum bed elevation) arises not from a slow down of the till velocity but from a change in deformable till thickness, A, due to changes in N.

The second objection is that it is observed at Mulajökull (which is a surging glacier) that, in the quiescent phase between surges, the effective pressure N is higher between the drumlins rather than lower, as the instability theory would suggest. This is indeed contradictory to the instability theory, but may be distracting because the surging appears to be fundamentally related to the process of drumlin growth. Indeed, it may be reasonable to suppose that surges are associated with a drainage switch between channels (with high N) in the quiescent phase and a distributed system (with low N) in the surge phase [61]. The instability theory in the form presented here does not address what would happen if a glacier is of surge type, nor indeed does it have anything to say about drumlin formation under temperate glaciers with copious water flow. It would of course be of interest to adapt the theory to confront the observations, but, from a theoretical perspective, that is an extremely ambitious task. To be fair, however, Menzies [25] also makes a similar comment, so it may be that this criticism is more widely valid.

5. Conclusion

We have presented the current edition of the instability theory of drumlin formation, and we have provided a numerical method which is able to solve it, although not presently sufficiently near actual parameter values. As we vary the critical parameters β, γ and δ, we find that bedforms of the correct size and elevation develop, that the solutions may be time-dependent over sufficiently long time scales that external ice sheet time dependence will have an effect, and that snapshots of bedforms resembling ribbed moraine, drumlins and lineations are all obtainable. These results open the way to a comparison with actual observed bedforms, although such a comparison is presently premature.

Data accessibility. The paper contains no additional data.

Authors' contributions. A.C.F. devised the project and wrote the paper. J.S.F. and I.R.M. constructed and solved the numerical model. All authors performed the literature review, and contributed to the analytic and numerical work. All authors worked on the final text.

Competing interests. We have no competing interests.

Funding. This publication has emanated from research conducted with the financial support of Science Foundation Ireland under grant nos. SFI/12/IA/1683 and SFI/13/IA/1923.

Acknowledgements. For continuing fruitful discussions, our thanks to Chris Clark, Chris Stokes, Jeremy Ely and Matteo Spagnolo.

References

1. Patterson CJ, Hooke LH. 1995 Physical environment of drumlin formation. *J. Glaciol.* **41**, 30–38. (doi:10.1017/S0022143000017731)
2. Pelletier JD. 2008 *Quantitative modeling of Earth surface processes*. Cambridge, UK: Cambridge University Press.
3. Clark CD. 2010 Emergent drumlins and their clones: from till dilatancy to flow instabilities. *J. Glaciol.* **51**, 1011–1025. (doi:10.3189/002214311796406068)
4. Hooke RLeB, Medford A. 2013 Are drumlins a product of a thermo-mechanical instability? *Quat. Res.* **79**, 458–464. (doi:10.1016/j.yqres.2012.12.002)
5. Fisher TG, Shaw J. 1992 A depositional model for Rogen moraine, with examples from the Avalon Peninsula, Newfoundland. *Can. J. Earth Sci.* **29**, 669–686. (doi:10.1139/e92-058)
6. Hättestrand C, Kleman J. 1999 Ribbed moraine formation. *Quat. Sci. Rev.* **18**, 43–61. (doi:10.1016/S0277-3791(97)00094-2)
7. Kleman J, Hättestrand C. 1999 Frozen-bed Fennoscandian and Laurentide ice sheets during the last glacial maximum. *Nature* **402**, 63–66. (doi:10.1038/47005)
8. Lindén M, Möller P, Adrielson L. 2008 Ribbed moraine formed by subglacial folding, thrust stacking and lee-side cavity infill. *Boreas* **37**, 102–131. (doi:10.1111/j.1502-3885.2007.00002.x)
9. Möller P. 2006 Rogen moraine: an example of glacial re-shaping of pre-existing landforms. *Quat. Sci. Rev.* **25**, 362–389. (doi:10.1016/j.quascirev.2005.01.011)
10. Möller P. 2010 Melt-out till and ribbed moraine formation, a case study from south Sweden. *Sediment. Geol.* **232**, 161–180. (doi:10.1016/j.sedgeo.2009.11.003)
11. Shaw J. 1983 Drumlin formation related to inverted melt-water erosional marks. *J. Glaciol.* **29**, 461–479. (doi:10.1017/S0022143000030367)
12. Shaw J. 1994 Hairpin erosional marks, horseshoe vortices and subglacial erosion. *Sediment. Geol.* **91**, 269–283. (doi:10.1016/0037-0738(94)90134-1)
13. Shaw J, Kvill D. 1984 A glaciofluvial origin for drumlins of the Livingstone Lake area, Saskatchewan. *Can. J. Earth Sci.* **21**, 1442–1459. (doi:10.1139/e84-150)
14. Shaw J, Sharpe DR. 1987 Drumlin formation by subglacial meltwater erosion. *Can. J. Earth Sci.* **24**, 2316–2322. (doi:10.1139/e87-216)
15. Shaw J, Rains B. 1989 Drumlins and catastrophic glacial floods. *Sediment. Geol.* **62**, 177–202. (doi:10.1016/0037-0738(89)90114-0)
16. Clark CD, Hughes ALC, Greenwood SL, Spagnolo M, Ng FSL. 2009 Size and shape characteristics of drumlins, derived from a large sample, and associated scaling laws. *Quat. Sci. Rev.* **28**, 677–692. (doi:10.1016/j.quascirev.2008.08.035)
17. Hall J. 1815 On the revolutions of the Earth's surface. *Trans. R. Soc. Edinb.* **7**, 169–184. (doi:10.1017/S0080456800019293)

18. Bryce J. 1833 On the evidences of diluvial action in the north of Ireland. *J. Geol. Soc. Dubl.* **1**, 34–44.
19. Kinahan GH, Close MH. 1872 *The general glaciation of Iar-Connaught and its neighbourhood, in the counties of Galway and Mayo*. Dublin, Ireland: Hodges, Foster and Co.
20. Tarr RS. 1894 The origin of drumlins. *Amer. Geol.* **10**, 339–362.
21. Millis J. 1911 What caused the drumlins? *Science* **34**, 60–62. (doi:10.1126/science.34.863.60)
22. Gravenor CP. 1953 The origin of drumlins. *Amer. J. Sci.* **251**, 674–681. (doi:10.2475/ajs.251.9.674)
23. Smalley IJ, Unwin DJ. 1968 The formation and shape of drumlins and their distribution and orientation in drumlin fields. *J. Glaciol.* **7**, 377–390. (doi:10.1017/S0022143000020591)
24. Boulton GS. 1987 A theory of drumlin formation by subglacial sediment deformation. In *Drumlin symposium* (eds J Menzies, J Rose), pp. 25–80. Rotterdam, The Netherlands: Balkema.
25. Menzies JM. 1979 The mechanics of drumlin formation with particular reference to the change in pore-water content of the till. *J. Glaciol.* **22**, 373–384. (doi:10.1017/S0022143000014349)
26. Menzies J. 1979 A review of the literature on the formation and location of drumlins. *Earth Sci. Rev.* **14**, 315–359. (doi:10.1016/0012-8252(79)90093-X)
27. Ely JC, Clark CD, Spagnolo M, Stokes CR, Greenwood SL, Hughes ALC, Dunlop P, Hess D. 2016 Do subglacial bedforms comprise a size and shape continuum? *Geomorphology* **257**, 108–119. (doi:10.1016/j.geomorph.2016.01.001)
28. Sugden DE, John BS. 1976 *Glaciers and landscape*. London, UK: Edward Arnold.
29. Fowler AC, Chapwanya M. 2014 An instability theory for the formation of ribbed moraine, drumlins and mega-scale glacial lineations. *Proc. R. Soc. A* **470**, 20140185. (doi:10.1098/rspa.2014.0185)
30. Iverson NR, McCracken RG, Zoet LK, Benediktsson ÍÖ, Schomacker A, Johnson MD, Woodard J. In press. A theoretical model of drumlin formation based on observations at Múlajökull. *J. G. R. Earth Surface*.
31. Hindmarsh RCA. 1998 The stability of a viscous till sheet coupled with ice flow, considered at wavelengths less than the ice thickness. *J. Glaciol.* **44**, 285–292. (doi:10.1017/S0022143000002628)
32. Fowler AC. 2000 An instability mechanism for drumlin formation. In *Deformation of subglacial materials* (eds A Maltman, MJ Hambrey, B Hubbard). Spec. Pub. Geol. Soc., vol. 176, pp. 307–319. London, UK: The Geological Society.
33. Dunlop P, Clark CD, Hindmarsh RCA. 2008 Bed ribbing instability explanation: testing a numerical model of ribbed moraine formation arising from coupled flow of ice and subglacial sediment. *J. Geophys. Res.* **113**, F03005. (doi:10.1029/2007JF000954)
34. Fowler AC. 2009 Instability modelling of drumlin formation incorporating lee-side cavity growth. *Proc. R. Soc. A* **465**, 2681–2702. (doi:10.1098/rspa.2008.0490)
35. Fowler AC. 2010 The instability theory of drumlin formation applied to Newtonian viscous ice of finite depth. *Proc. R. Soc. A* **466**, 2673–2694. (doi:10.1098/rspa.2010.0017)
36. Fowler AC. 2010 The formation of subglacial streams and mega-scale glacial lineations. *Proc. R. Soc. A* **466**, 3181–3201. (doi:10.1098/rspa.2010.0009)
37. Kyrke-Smith TM, Fowler AC. 2014 Subglacial swamps. *Proc. R. Soc. A* **470**, 20140340. (doi:10.1098/rspa.2014.0340)
38. Chapwanya M, Clark CD, Fowler AC. 2011 Numerical computations of a theoretical model of ribbed moraine formation. *Earth Surf. Process. Landf.* **36**, 1105–1112. (doi:10.1002/esp.2138)
39. Stokes CR, Fowler AC, Clark CD, Hindmarsh RCA, Spagnolo M. 2013 The instability theory of drumlin formation and its explanation of their varied composition and internal structure. *Quat. Sci. Rev.* **62**, 77–96. (doi:10.1016/j.quascirev.2012.11.011)
40. Smith TR, Bretherton FP. 1972 Stability and the conservation of mass in drainage basin evolution. *Water Resour. Res.* **8**, 1506–1529. (doi:10.1029/WR008i006p01506)
41. Willgoose G, Bras RL, Rodríguez-Iturbe I. 1991 A coupled channel network growth and hillslope evolution model: I. *Theory Water Resour. Res.* **27**, 1671–1684. (doi:10.1029/91WR00935)
42. Kramer S, Marder M. 1992 Evolution of river networks. *Phys. Rev. Lett.* **68**, 205–208. (doi:10.1103/PhysRevLett.68.205)
43. Tucker GE, Slingerland RL. 1994 Erosional dynamics, flexural isostasy, and long-lived escarpments: a numerical modeling study. *J. Geophys. Res.* **99**, 12 229–12 243. (doi:10.1029/94JB00320)
44. Barchyn TE, Dowling TPF, Stokes CR, Hugenholtz CH. 2016 Subglacial bedform morphology controlled by ice speed and sediment volume. *Geophys. Res. Lett.* **43**, 7572–7580. (doi:10.1002/2016GL069558)

45. Creyts TT, Schoof CG. 2009 Drainage through subglacial water sheets. *J. Geophys. Res.* **114**, F04008. (doi:10.1029/2008JF001215)
46. Goodwin ID. 1988 The nature and origin of a Jökulhlaup near Casey Station, Antarctica. *J. Glaciol.* **34**, 95–101. (doi:10.1017/S0022143000009114)
47. Engelhardt H, Kamb B. 2013 Kamb Ice Stream flow history and surge potential. *Ann. Glaciol.* **54**, 287–298. (doi:10.3189/2013AoG63A535)
48. Sergienko OV, Hulbe CL. 2011 'Sticky spots' and subglacial lakes under ice streams of the Siple Coast, Antarctica. *Ann. Glaciol.* **52**, 18–22. (doi:10.3189/172756411797252176)
49. Röthlisberger H. 1972 Water pressure in intra- and subglacial channels. *J. Glaciol.* **11**, 177–203. (doi:10.1017/S0022143000022188)
50. Nye JF. 1976 Water flow in glaciers: Jökulhlaups, tunnels, and veins. *J. Glaciol.* **17**, 181–207. (doi:10.1017/S002214300001354X)
51. Smith JD. 1970 Stability of a sand bed subjected to a shear flow of low Froude number. *J. Geophys. Res.* **75**, 5928–5940. (doi:10.1029/JC075i030p05928)
52. Engelund F. 1970 Instability of erodible beds. *J. Fluid Mech.* **42**, 225–244. (doi:10.1017/S0022112070001210)
53. Loewenherz DS. 1991 Stability and the initiation of channelized surface drainage: a reassessment of the short wavelength limit. *J. Geophys. Res.* **96**, 8453–8464. (doi:10.1029/90JB02704)
54. Loewenherz-Lawrence DS. 1994 Hydrodynamic description for advective sediment transport processes and rill initiation. *Water Resour. Res.* **30**, 3203–3212. (doi:10.1029/94WR02076)
55. Fowler AC, Kopteva N, Oakley C. 2007 The formation of river channels. *SIAM J. Appl. Math.* **67**, 1016–1040. (doi:10.1137/050629264)
56. Meier SW, Melani Barreiro DA, Ottino JM, Lueptow RM. 2008 Coarsening of granular segregation patterns in quasi-two-dimensional tumblers. *Nat. Phys.* **4**, 244–248. (doi:10.1038/nphys881)
57. Schoof C. 2007 Pressure-dependent viscosity and interfacial instability in coupled ice-sediment flow. *J. Fluid Mech.* **570**, 227–252. (doi:10.1017/S0022112006002874)
58. Schoof C. 2007 Cavitation in deformable glacier beds. *SIAM J. Appl. Math.* **67**, 1633–1653. (doi:10.1137/050646470)
59. Spagnolo M, Clark CD, Hughes ALC. 2012 Drumlin relief. *Geomorphology* **153–154**, 179–191. (doi:10.1016/j.geomorph.2012.02.023)
60. McCracken RG, Iverson NR, Benediktsson ÍÖ, Schomacker A, Zoet LK, Johnson MD, Hooyer TS, Ingólfsson Ó. 2016 Origin of the active drumlin field at Múlajökull, Iceland: new insights from till shear and consolidation patterns. *Quat. Sci. Rev.* **148**, 243–260. (doi:10.1016/j.quascirev.2016.07.008)
61. Fowler AC. 1987 A theory of glacier surges. *J. Geophys. Res.* **92**, 9111–9120. (doi:10.1029/JB092iB09p09111)